

# Green Chemistry

Accepted Manuscript



This article can be cited before page numbers have been issued, to do this please use: X. Kong, R. Zheng, Y. Zhu, G. Ding, Y. L. Zhu and Y. Li, *Green Chem.*, 2015, DOI: 10.1039/C5GC00062A.



This is an *Accepted Manuscript*, which has been through the Royal Society of Chemistry peer review process and has been accepted for publication.

*Accepted Manuscripts* are published online shortly after acceptance, before technical editing, formatting and proof reading. Using this free service, authors can make their results available to the community, in citable form, before we publish the edited article. We will replace this *Accepted Manuscript* with the edited and formatted *Advance Article* as soon as it is available.

You can find more information about *Accepted Manuscripts* in the [Information for Authors](#).

Please note that technical editing may introduce minor changes to the text and/or graphics, which may alter content. The journal's standard [Terms & Conditions](#) and the [Ethical guidelines](#) still apply. In no event shall the Royal Society of Chemistry be held responsible for any errors or omissions in this *Accepted Manuscript* or any consequences arising from the use of any information it contains.

## ARTICLE

# Rational Design of Ni-based Catalysts derived from Hydrotalcite for Selective Hydrogenation of 5-Hydroxymethylfurfural

Cite this: DOI: 10.1039/x0xx00000x

Xiao Kong,<sup>a, b</sup> Runxiao Zheng,<sup>c</sup> Yifeng Zhu,<sup>a, b</sup> Guoqiang Ding,<sup>d</sup> Yulei Zhu<sup>\*a, d</sup> and Yong-Wang Li<sup>a, d</sup>

Received 00th January 2012,  
Accepted 00th January 2012

DOI: 10.1039/x0xx00000x

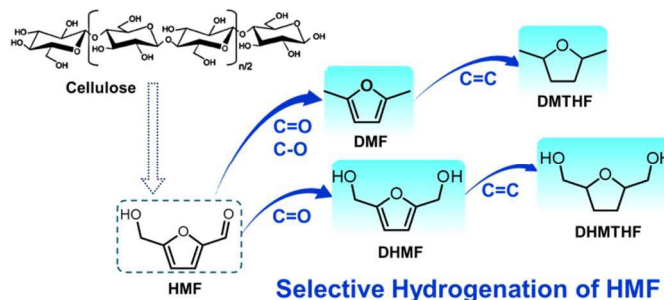
www.rsc.org/

Selective hydrogenation of 5-hydroxymethylfurfural (HMF) is of great importance for future energy and chemical supply. Herein, we propose for the first time that non-noble Ni-Al<sub>2</sub>O<sub>3</sub> catalysts derived from hydrotalcite-like compounds can efficiently and selectively convert HMF to 2,5-dimethylfuran (DMF), 2,5-dimethyltetrahydrofuran (DMTHF) and 2,5-dihydroxymethyltetrahydrofuran (DHMTHF). Homogeneous elemental distributions of hydrotalcite-like precursor facilitate the good dispersion of Ni and Al<sub>2</sub>O<sub>3</sub> species and strong interaction between them over the resulted catalysts. The catalysts therefore exhibited superior reactivity. Through fine modulation of surface metal-acid bifunctional sites and control of reaction conditions, high yields of DMF (91.5%), DMTHF (97.4%) and DHMTHF (96.2%) can be diversely achieved. The results demonstrate the feasibility of Ni catalysts for selective hydrogenation of C=O, C=C and C-O bonds, which have great potential for biomass utilization.

## Introduction

With the shrinking of fossil resources, biomass is considered to be an ideal substitute in the production of chemicals and fuels.<sup>1</sup> Biomass, especially the inedible lignocellulose, mainly composed of cellulose, hemicellulose and lignin, of which cellulose is the major component (~35 to 50%).<sup>2</sup> 5-hydroxymethylfurfural (HMF) is an important platform chemical, which can be facilely obtained from abundant cellulose using acid catalysts.<sup>3,4</sup> The C=O, C-O, C=C and furan ring of HMF make it flexible for further catalytic transformations by various methodologies (e.g., hydrogenation<sup>4,5</sup>, oxidation<sup>6</sup>, decarbonylation<sup>7</sup>, etherification<sup>8</sup>). Thus, the catalytic conversion of HMF is a key step in cellulosic biomass utilizations. The products from selective hydrogenation of HMF can be grouped into two main categories. One is the promising biofuel with high energy densities and octane numbers, including 2,5-dimethylfuran (DMF) and 2,5-dimethyltetrahydrofuran (DMTHF) (Scheme 1).<sup>9-12</sup> Reducing the O-content of HMF via hydrogenolysis is the major intention for biofuel production.<sup>1</sup> Another category is the diol precursor for polymer production, such as 2,5-dihydroxymethylfuran (DHMF) and 2,5-dihydroxymethyltetrahydrofuran (DHMTHF) (Scheme 1).<sup>13,14</sup> For the synthesis of diols (e.g., DHMTHF), the hydrogenation of unsaturated C=O/C=C bonds needs to be promoted while excessive hydrogenolysis of hydroxymethyl should be suppressed.

Yet, one common impediment for selective hydrogenation of HMF (e.g., HMF to DMF/DHMF) is the usage of noble metal catalysts. To produce DMF, a CuRu/C catalyst was firstly proposed with a yield of 76~79%.<sup>9</sup> After this work, studies



**Scheme 1** Hydrogenation of HMF to various products.

mainly focused on the noble metal catalysts (e.g., Pt<sup>10,15</sup>, Ru<sup>9,16</sup>, Pd<sup>17</sup>). However, the availability and high price greatly hindered the commercial applications of noble metals. The development of non-noble substitutes therefore received great interests for both academic and industrial purposes.<sup>18,19</sup> Recently, a bifunctional Ni-W<sub>2</sub>C/AC catalyst was proposed for DMF synthesis with high yield<sup>19</sup>, indicating the potential of non-noble catalysts. In our previous work<sup>20</sup>, a switchable synthesis of DMF and DHMTHF was achieved with high yield respectively over Raney Ni, demonstrating high feasibility of Ni-based catalyst. Nevertheless, large amounts of Ni catalysts were used in both works to guarantee the high HMF conversion, revealing that the efficiency of non-noble catalysts needed to be improved. For DMTHF synthesis, Sen et al.<sup>11,12</sup> reported that DMTHF could be obtained directly from hexose using homogeneous RhCl<sub>3</sub>/HI system, while few reports exist

on HMF hydrogenation to DMTHF. DHMTHF could be produced with high yields (generally above 90%) by HMF hydrogenation. However, noble metals were also frequently used (e.g., Ru<sup>14, 21</sup>, Pd<sup>13, 22</sup>). Thus, the development of efficient non-noble catalysts plays a key role for HMF hydrogenation.

Another challenge for upgrading HMF is the poor selectivity of products. Due to various functional groups (C=O, C=C, C-O and furan ring) of HMF, the product of HMF hydrogenation is usually a mixture of many compounds (e.g., ring-hydrogenated compounds and side chain hydrogenation/hydrogenolysis products). Hydrogenation of HMF to DMF involves C=O hydrogenation and subsequent C-O hydrogenolysis while synthesis of DMTHF needs to further saturate the furan ring. In contrast, synthesis of DHMTHF involves the hydrogenation of unsaturated bonds (C=O and C=C bonds), for which the hydrogenolysis of C-O bonds should be suppressed. Considering the different intentions, the desired active sites for the synthesis of DMF/DMTHF and DHMTHF are different. The former usually needs balanced metal-acid sites<sup>19</sup> and the latter requires highly dispersed metal sites with little acid sites<sup>21</sup>. In many cases, the specific catalyst with a fixed composition can only satisfy a certain type of reaction. Herein, we demonstrate how to modulate the surface active sites (metal and acid sites) over a typical catalyst (e.g., Ni-Al<sub>2</sub>O<sub>3</sub> catalyst with a fixed composition) to obtain the desired products by the control of calcination procedure. Besides, because of the high boiling point of HMF (291 °C), the hydrogenation reactions were usually carried out in liquid phases and harsh conditions (e.g., high-temperatures).<sup>23</sup> The stability of catalyst should also be concerned.

In view of the above problems, rational design of a cheap, highly reactive and selective catalyst for HMF hydrogenation is important. In this paper, we propose for the first time that hydrotalcite derived Ni-Al<sub>2</sub>O<sub>3</sub> catalysts can selectively catalyze conversion of HMF into DMF, DMTHF and DHMTHF with high yields (91.5%, 97.4% and 96.2% respectively). The hydrotalcite-like precursor, with general formula [M<sup>2+</sup><sub>1-x</sub>M<sup>3+</sup><sub>x</sub>(OH)<sub>2</sub>]<sup>x+</sup>A<sup>z-</sup><sub>z/2</sub>·mH<sub>2</sub>O (M<sup>2+</sup> = Ni<sup>2+</sup>, M<sup>3+</sup> = Al<sup>3+</sup>, A<sup>z-</sup> = CO<sub>3</sub><sup>2-</sup> in our case), was prepared by a facile and simple constant-pH coprecipitation. Uniform and well-organized Ni/Al distributions of the precursor lead to highly dispersed Ni and Al<sub>2</sub>O<sub>3</sub> species; and thus a superior activity was achieved. By means of annealing at different temperatures, the surface metallic Ni and acid sites over the resulted catalysts can be finely modulated, as a comprehensive result of tuned dispersion, reducibility and Ni-Al<sub>2</sub>O<sub>3</sub> interactions. Finally, through modulation of surface active sites and reaction conditions, the selective conversions of HMF toward products can be tailored according to the different requirements of reactions. Besides, the strong interactions of Ni-Al<sub>2</sub>O<sub>3</sub> species could benefit the catalyst stability. We not only describe the selective conversion of HMF over base metal Ni catalyst but also present a catalyst design strategy for selective conversion of C=O, C=C, C-O bonds.

## Results and discussion

### Characterizations of Ni-Al hydrotalcite-like precursor and calcined catalysts

The hydrotalcite-like precursor (NiAl-HT) was prepared by a constant-pH co-precipitation. Upon calcination at different temperatures, the NiAl-CT (CT indicates the calcination temperature) catalysts were obtained. To investigate the decomposition process during calcination, thermo-gravimetry

(TG) experiment of NiAl-HT was performed under air atmosphere (**Figure 1**). The weight loss between 30 and 200 °C corresponded to the removal of physically adsorbed water and interlayer water, which was in accordance with the previous reports.<sup>24, 25</sup> The rapid weight loss around 328 °C could be attributed to the concomitant dehydroxylation of the laminae and expulsion of the carbonate anions (in the form of CO<sub>2</sub>) located in the interlayer regions.<sup>24</sup> According to Bonura et al.,<sup>26</sup> the release of CO<sub>2</sub> during the calcination process could hinder the sintering of the oxide components. By further raising the temperature above 400 °C, slight weight loss was detected, indicating that the decomposition process completed and the NiAl-HT precursor was converted into oxide composites totally.

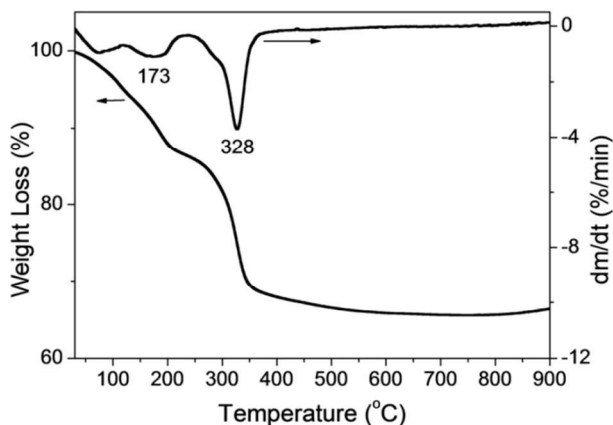


**Figure 1** TG curves of NiAl precursor (NiAl-HT).

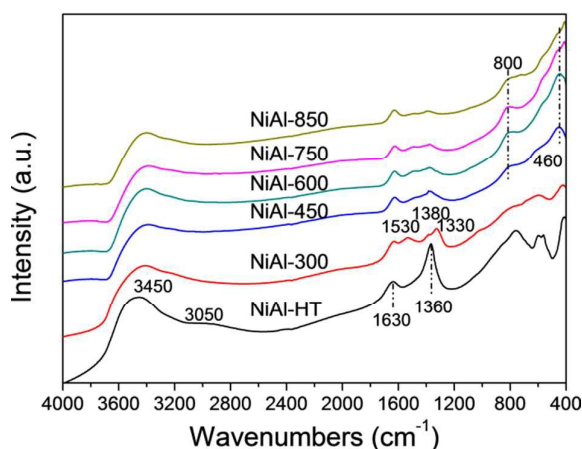
IR spectra visualized the decomposition process of NiAl-HT precursor upon calcination (**Figure 2**). For NiAl-HT sample, the bands at 3450 cm<sup>-1</sup> and 1630 cm<sup>-1</sup> are the characteristics of HOH bending vibration of physically adsorbed water.<sup>27</sup> The shoulder band at 3050 cm<sup>-1</sup> is induced by hydrogen bonding of H<sub>2</sub>O to CO<sub>3</sub><sup>2-</sup> ions in the interlayer space.<sup>27</sup> The band around 1360 cm<sup>-1</sup> is attributed to ν<sub>3</sub> vibration of the carbonate.<sup>27, 28</sup> For NiAl-300 catalyst, the shoulder band at 3050 cm<sup>-1</sup> diminished, indicating the removal of interlayer water. The ν<sub>3</sub> mode of the carbonate splitted into new bands at 1330, 1380 and 1530 cm<sup>-1</sup>, indicating the reorganization of carbonate anions after calcination at 300 °C. The band at 1330 cm<sup>-1</sup> is the vibrations of C-O band interacted with OH groups of the layers. Further increase of calcination temperature resulted in the disappearance of 1330 cm<sup>-1</sup>, indicating dehydroxylation of the laminae process. The bands at 1380 and 1530 cm<sup>-1</sup> are related to the carbonates coordinated to the metal ions and the C=O vibration in CO<sub>3</sub><sup>2-</sup> anions respectively. The intensity of both bands decreased rapidly upon increasing the calcination temperatures, indicating the removal of carbonate species. For NiAl-850 catalyst, only slight peaks associated with carbonates were observed. The IR spectra revealed the removal of interlayer water, hydroxyl and carbonate groups upon calcination, which fitted well with the TG results. The information about states of Ni<sup>2+</sup> and Al<sup>3+</sup> species over the calcined catalyst can also be derived from the IR results, which would be revealed in the following parts.

The above results showed that the lamellar structure of NiAl-300 catalyst collapsed partially whereas the structure disappeared completely for the NiAl-CT catalysts calcined at higher temperatures. The different calcination temperature

**Table 1** Main physicochemical properties of NiAl-HT and NiAl-CT catalysts.

Sample	Ni/Al ratio (mol/mol) <sup>a</sup>	S <sub>BET</sub> (m <sup>2</sup> /g) <sup>b</sup>	V <sub>p</sub> (cm <sup>3</sup> /g) <sup>b</sup>	d <sub>p</sub> (nm) <sup>b</sup>	d <sub>NiO</sub> (nm) <sup>c</sup>	d <sub>Ni</sub> (nm) <sup>d</sup>	Amounts of Ni sites (mmol/g <sub>cat.</sub> ) <sup>e</sup>	Amounts of acid sites (μmol NH <sub>3</sub> /g <sub>cat.</sub> ) <sup>f</sup>
NiAl-HT	2.93	79	0.12	3.8	-	-	-	-
NiAl-300	2.90	183	0.39	6.1	-	3.7	2.4	1.1
NiAl-450	2.90	200	0.34	5.2	3.0	3.7	2.3	1.7
NiAl-600	2.89	162	0.35	6.4	3.5	4.0	1.2	1.9
NiAl-750	2.90	143	0.34	6.9	4.1	4.8	0.4	2.1
NiAl-850	2.90	123	0.35	8.3	5.1	5.3	0.3	2.2

<sup>a</sup> Ni/Al ratios were determined by ICP experiments. <sup>b</sup> The BET surface area, pore volume and pore size were determined by N<sub>2</sub> physical adsorption. <sup>c</sup> calculated by NiO (200) reflection (2θ=43.3°) based on Scherrer equation. <sup>d</sup> calculated by Ni (200) reflection (2θ=51.8°) based on Scherrer equation. <sup>e</sup> Amounts of metal sites were determined by H<sub>2</sub>-TPD. <sup>f</sup> Amounts of acid sites were determined by NH<sub>3</sub>-TPD.

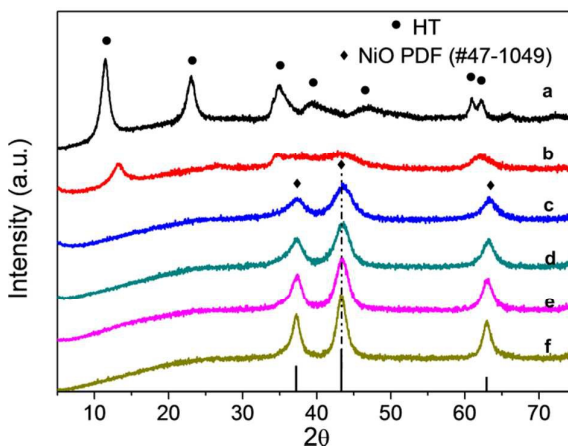
**Figure 2** FT-IR spectra of NiAl-HT and NiAl-CT.

would be expected to have great effects on the dispersion, reducibility, acid properties and NiO-Al<sub>2</sub>O<sub>3</sub> interactions; and thus lead to different surface sites over the resulted catalysts.

The physicochemical and surface properties of NiAl-HT precursor and NiAl-CT catalysts are summarized in **Table 1**. ICP results showed that Ni/Al ratios of all the catalysts were close to the nominal value of 3.0. The specific BET surface area of the NiAl-HT precursor was 79 m<sup>2</sup>/g. Raising calcination temperature in the range of 60 to 450 °C resulted in the gradual increase of BET surface area from 79 to 200 m<sup>2</sup>/g. The increase was related to the release of H<sub>2</sub>O and CO<sub>2</sub><sup>29</sup>, which was in good accordance with TG/IR results. The calcination treatment also resulted in an increase of the pore size and pore volume. Further elevation of calcination temperature caused the decrease in BET surface area, indicating that sintering of oxidic components occurred. Upon reduction, the NiAl-CT catalysts exhibited different amounts of surface metal and acid sites (**Table 1**). The results showed a decrease of surface metallic Ni concentrations and an increase of amounts of surface acid sites with the elevation of calcination temperature.

**Figure 3** shows the XRD patterns of NiAl-HT and calcined NiAl-CT catalysts. Evident peaks at 11.7°, 23.6°, 35.0°, 39.7°, 47.1°, 60.9° and 62.4° were observed for NiAl-HT precursor, which belong to diffractions of lamellar structure of hydrotalcite. Upon calcination at 300 °C, the peak at 11.7° broadened and some peaks disappeared, confirming that the hydrotalcite structure was partially destroyed, as revealed in TG and IR results. No characteristics of hydrotalcite were

observed over the catalysts calcined at temperatures above 300 °C, indicating the total decomposition of NiAl-HT precursor. In contrast, the peaks at 37.2°, 43.3° and 62.9° emerged over the patterns of NiAl-CT catalysts (CT >300 °C), which can be attributed to the diffractions of NiO phase. The standard diffractogram of NiO (PDF#47-1049) is sketched as bars at the bottom of **Figure 3**. The results demonstrated the transformation of NiAl-HT precursor into oxide compounds. No diffraction peak related to Al<sub>2</sub>O<sub>3</sub> was observed, revealing the X-ray amorphous state of Al<sub>2</sub>O<sub>3</sub>. The peaks of NiO intensified slightly with the increase of calcination temperature, indicating a slow particle growth of NiO. We calculated the particle size of NiO by Scherrer equation (**Table 1**). Although it increased slightly with the calcination temperature, the particle size of NiO over the NiAl-CT catalysts was small. NiAl-850 catalyst exhibited the largest particle size (~5.1nm), despite of the high temperature treatment. One important reason for the high dispersion of NiO is that the Ni<sup>2+</sup> and Al<sup>3+</sup> were distributed at atomic levels in hydrotalcite structure. The enhanced interactions between NiO and Al<sub>2</sub>O<sub>3</sub> species were also responsible for the highly dispersed NiO particles and the resistance of NiO against sintering when the catalysts were calcined at high temperatures. Clause et al.<sup>24</sup> reported that the Al-containing phases interacted strongly with NiO species and could stabilize the NiO species for hydrotalcite-derived samples. Thus, no obvious sintering of NiO particles was observed with the increase of calcination temperature.

**Figure 3** XRD patterns of NiAl-HT and NiAl-CT (a, NiAl-HT; b, NiAl-300; c, NiAl-450; d, NiAl-600; e, NiAl-750; f, NiAl-850. HT: hydrotalcite.).

To determine the nature and chemical state of Ni<sup>2+</sup> and Al<sup>3+</sup> species over the calcined samples, Raman and IR experiments were performed (Figure 4 and Figure 2). Raman bands at 150 cm<sup>-1</sup>, 482 cm<sup>-1</sup> and 545 cm<sup>-1</sup> are all related to vibrations of Ni-Al hydrotalcite-like structure. These bands diminished upon calcination, indicating the decomposition of NiAl-HT precursor.<sup>27</sup> As reported in previous works<sup>30</sup>, crystalline NiO exhibits two broad bands at 460 and 500 cm<sup>-1</sup> while crystalline NiAl<sub>2</sub>O<sub>4</sub> spinel possesses characteristic band located at 600 cm<sup>-1</sup>. However, a single band around 550 cm<sup>-1</sup> was observed in our case, which was different from the Raman bands of crystalline NiO and NiAl<sub>2</sub>O<sub>4</sub>. According to J. Pérez-Ramírez et al.<sup>27</sup>, the band at 550 cm<sup>-1</sup> can be assigned to a surface Ni oxide component with Ni<sup>2+</sup> incorporated into the subsurface of the alumina support, indicating the strong interactions between NiO and Al<sub>2</sub>O<sub>3</sub>. For the catalysts calcined at high temperatures (e.g., 850 °C), the band broadened and shifted significantly to higher peak around 600 cm<sup>-1</sup>, revealing the enhanced metal support interactions. The strong interactions could stabilize the NiO particles and prevent the sintering of NiO, as evidenced by the XRD results.

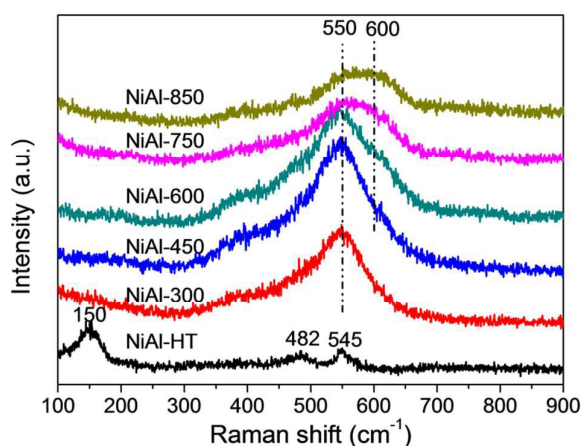


**Figure 4** Raman spectra of the NiAl-HT and NiAl-CT catalysts.

IR results confirmed the chemical states change of Ni and Al species over the NiAl-CT catalysts, as evidenced in Raman results. The  $\nu$  Ni-O arised from NiO<sub>6</sub> can be found at 400 cm<sup>-1</sup>. The band around 460 cm<sup>-1</sup> was an “average” band between the stretching vibration of octahedral AlO<sub>6</sub> and that of octahedral NiO<sub>6</sub>.<sup>28</sup> The adsorption band in the range of 700–800 cm<sup>-1</sup> was assigned to the stretching vibrations of the isolated tetrahedral AlO<sub>4</sub>.<sup>27, 28, 31</sup> With increase of calcination temperature (especially for 850 °C), the vibrations of AlO<sub>4</sub> intensified and broadened due to the structure change from AlO<sub>6</sub> to AlO<sub>4</sub> atomic group.<sup>31</sup> The structure change of Al<sup>3+</sup> can be related to the strong interactions between Ni<sup>2+</sup> and Al<sup>3+</sup> species.<sup>32</sup> The Raman and IR results both suggested that the NiO was strongly interacting with the emerging alumina support upon hydrotalcite decomposition and the strong interactions were greatly enhanced after calcination.

To further investigate the structural evolution, interaction between NiO and Al<sub>2</sub>O<sub>3</sub> and the reducibility of catalysts, TPR experiments were performed (Figure 5). NiAl-300 catalyst exhibited two hydrogen consumption peaks, indicating the existence of two different kinds of Ni species. Combined with the above results (TG, IR and XRD), the first shoulder peak of NiAl-300 was ascribed to the reduction of Ni<sup>2+</sup> species in lamellar structure and the main reduction peak was assigned to the reduction of NiO in interaction with Al<sub>2</sub>O<sub>3</sub>, which is in

accordance with previous report.<sup>33, 34</sup> The NiAl-CT catalysts annealed at higher temperatures (450, 600, 750 and 850 °C) all exhibited broad reduction profiles which could be attributed to the reduction of NiO species. With the increase of calcination temperature, the peak shifted toward higher temperature. One reason for the migration of reduction temperature is the slightly increased NiO particle sizes, as evidenced by the XRD results.<sup>35</sup> According to the Raman and IR results, the interactions between NiO and Al<sub>2</sub>O<sub>3</sub> were greatly promoted when the calcination temperature was increased. Considering the slight discrepancy of NiO particle sizes and the significantly different reduction profiles, the main factor for the hindered reduction could be attributed to the enhanced interactions between NiO and Al<sub>2</sub>O<sub>3</sub> species.<sup>29, 34</sup> For a NiAl-CT catalyst, the higher reduction temperature indicated the lower reducibility under a certain H<sub>2</sub>-pretreatment and the fewer surface metallic Ni sites. Thus, the surface metal sites could be modulated by tuning the calcination temperature, NiO-Al<sub>2</sub>O<sub>3</sub> interactions and reducibility.

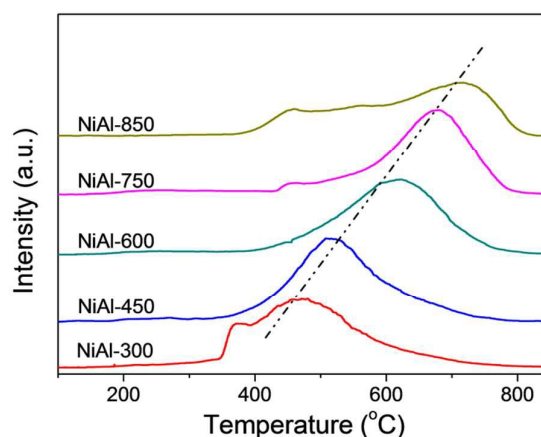


**Figure 5** H<sub>2</sub>-TPR results of NiAl-CT catalysts.

All the above results indicated that the hydrotalcite structure was decomposed and metal oxide was formed with increase of calcination temperature. The derived catalysts have been demonstrated to possess highly dispersed Ni particles and strong interactions between NiO and Al<sub>2</sub>O<sub>3</sub>, which are desired features of an efficient catalyst for HMF hydrogenation. The increased calcination temperature further enhanced the metal support interactions and also hindered the reduction process.

#### Characterizations of reduced catalysts

**Figure 6** shows the XRD patterns of reduced NiAl-CT catalysts. All the catalysts exhibited broad peaks at 44.5° and 51.8°, which belong to the characteristics of metallic Ni phase (PDF#04-0850). These peaks of Ni intensified slightly with increase of calcination temperature. For those catalysts calcined at high temperatures (NiAl-600, NiAl-750, NiAl-850), the remnant peaks of NiO at 37.2°, 43.3° and 62.9° were also observed. This is because of the hindered reducibility, as a result of both enhanced NiO-Al<sub>2</sub>O<sub>3</sub> interactions and slightly increased particle sizes of NiO. The tuned reducibility of catalysts would thus greatly influence the amounts of total metallic Ni sites over the surface. Because the peak of Ni (111) at 44.5° was greatly overlapped with that of NiO (200), the Ni particle sizes were calculated by Ni (200) reflection (2 $\theta$ =51.8°) based on Scherrer equation (Table 1). With the increase of calcination temperature, the half-peak width decreased

slightly, indicating a slow increase of Ni particle size (from 3.7 to 5.3 nm). The slight increase of Ni particle sizes suggested a limited sintering of Ni nanoparticles at high temperature because of the strong interaction between Ni and Al<sub>2</sub>O<sub>3</sub>. The TEM images (**Figure S1**) further illustrated the microstructures of reduced NiAl-CT catalysts. For reduced NiAl-300 and NiAl-450, highly dispersed and rounded nanoparticles with diameter of 3-10 nm are distributed in the amorphous Al<sub>2</sub>O<sub>3</sub> matrix. With the increase of calcination temperature, the particles grew slightly and changed into nodular particles. Nevertheless, the catalysts possessed relatively small particles even after high temperature calcination.

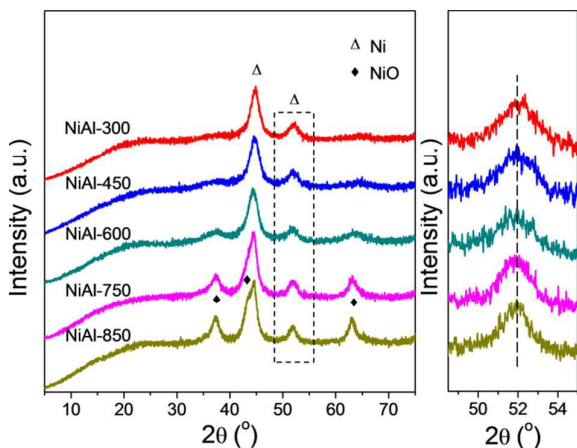
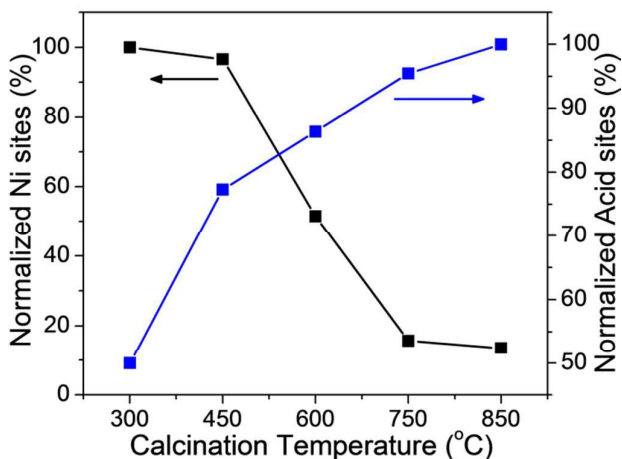


**Figure 6** XRD patterns of reduced NiAl-CT catalysts

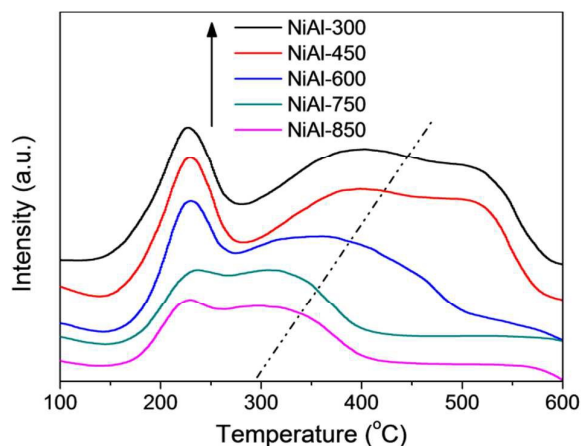
To quantitatively determine the amount of surface metallic Ni and acid sites over the reduced catalysts, H<sub>2</sub>-TPD (**Figure S2**) and NH<sub>3</sub>-TPD (**Figure S3**) measurements were thus performed. Similar amounts of Ni sites were obtained over NiAl-450 and NiAl-300 catalysts. Calcination at higher temperatures decreased the number of surface Ni<sup>0</sup> sites rapidly. The NiAl-850 catalyst possessed the lowest amount of Ni<sup>0</sup> sites because of the depressed reducibility and dispersion. **Figure S3** showed the surface acidity of NiAl-CT catalysts. All the catalysts exhibited similar acid strength while showed different density of surface acid sites. The density of acid sites increased gradually with the elevation of calcination temperature. The surface acidity was associated with Al<sup>3+</sup> species and could be attributed to the dehydration of surface hydroxyl groups.<sup>35, 36</sup> Upon calcination, the dehydration process would result in some freed and defective Al<sup>3+</sup> sites; and thus the amount of surface acid sites increased. The enhanced surface acidity amounts would greatly benefit for the C-O hydrogenolysis reactions.<sup>32, 35, 37</sup>

The amounts of surface metallic Ni and acid sites are listed in **Table 1**. **Figure 7** illustrated the relationship between the normalized concentrations of surface metallic Ni/acid sites and calcination temperature. The balance of surface metal and acid sites was greatly tuned by calcination temperature. For the catalyst calcined at low temperature (e.g., NiAl-300), high concentration of metallic Ni sites and low amount of acid sites were obtained. When the catalysts were annealed at higher temperatures (e.g., 450 and 600 °C), the evolutions of surface and structural properties induced more acid sites while the decreased reducibility lead to the decline of Ni sites. The calcination at 750 and 850 °C further decreased the amounts of surface metallic Ni sites, due to the greatly enhanced NiO-Al<sub>2</sub>O<sub>3</sub> interactions, depressed reducibility and slightly increased NiO particle sizes. The results showed that the

surface Ni-acid sites over the NiAl-CT catalysts with a fixed composition can be finely modulated via a simple calcination treatment at different temperatures, which were expected to have different reactivity for selective hydrogenation of HMF.



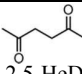





**Figure 7** The normalized Ni and acid sites of reduced NiAl-CT catalysts. (Normalized: the highest is 100%)



**Figure 8** CO-TPD spectra of NiAl-CT catalysts

CO-TPD was also performed to probe the interactions between Ni and Al<sub>2</sub>O<sub>3</sub> species over reduced catalysts. As shown in **Figure 8**, all catalysts exhibited two CO peaks at 200-250 °C and 300-600 °C, which can be described as the contribution of molecularly adsorbed CO on smooth crystal planes and recombination of dissociated C and O species on stepped Ni surfaces respectively.<sup>38</sup> With the increase of calcination temperature, the CO uptakes decreased, indicating the decrease of active sites, which was in accordance with H<sub>2</sub>-TPD results. Moreover, a shift of the peak around 300-600 °C to low temperature was observed, revealing weaker CO-catalyst interactions over the catalysts calcined at high temperatures. The shift was diagnostic of an electron-deficient state of Ni sites. This is because that the metal of rich electron could strengthen the C-metal bond and weaken the C-O bond, enabling a dissociation of CO.<sup>39, 40</sup> Therefore, the lower desorption temperature of CO over high-temperature calcined catalysts was indicative of strong metal support interactions, which is in accordance with the previous reports.<sup>40</sup> The strong interactions between Ni and Al<sub>2</sub>O<sub>3</sub> could be helpful for the metal stability against sintering in liquid phase.

**Table 2** Hydrogenation of HMF over NiAl-CT catalysts.<sup>a</sup>

Catalyst	Conv. %	Sel. %						Others
								
NiAl-850	100	3.2	1.4	91.5	3.6	0	0	0.3
NiAl-750	100	3.4	9.5	80.1	4.9	0	0	2.1
NiAl-600	100	0	25.4	66.4	3.1	2.8	0	2.3
NiAl-450	100	0	27.3	62.0	4.5	2.8	0	3.4
NiAl-300	100	0	11.0	44.6	4.9	11.8	20.2	7.5

<sup>a</sup> Reaction conditions: 1.2 MPa, 180 °C, 4 h, HMF 1.5 g, 1,4-dioxane 35 ml, catalyst 0.1 g. Others mainly include 5-methylfurfural and C-C cracking products.

### Selective hydrogenation of HMF

Our contribution marks at least the following desirable features: (1) the homogeneous element distributions of hydrotalcite precursor facilitated the highly dispersed Ni and Al<sub>2</sub>O<sub>3</sub> species, as well as the strong interactions between them; (2) the balance of surface metallic Ni and acid sites can be finely modulated by calcination at different temperatures; (3) the high temperature calcination also enhanced the interactions between Ni and Al<sub>2</sub>O<sub>3</sub> species. The selectivity of desired products from HMF hydrogenation can be greatly influenced by the different reactivity of catalysts towards different functional groups (C=O, C-O and C=C bonds). DMF, DMTHF and DHMTHF (Scheme 1) can be tunably synthesized by the control of reaction conditions and fine manipulation of metal-acid sites over NiAl-CT catalyst.

### Synthesis of DMF by HMF hydrogenation

DMF production from HMF hydrogenation is composed of two main steps: the hydrogenation of aldehyde group and the subsequent hydrogenolysis of hydroxymethyl groups. DHMF and 5-methylfurfuryl alcohol (MFA) are the key intermediates for this reaction.<sup>20</sup> The excessive conversion of DMF would generate some byproducts including DMTHF and 2,5-hexanedione (2,5-HeD). Table 2 presents the catalytic performance of NiAl-CT catalysts for DMF synthesis. The reaction was performed at 180 °C, which was screened as an optimal temperature for DMF synthesis in our previous work.<sup>20</sup> HMF was totally converted over all the catalysts after 4 h, indicating the high reactivity of non-noble NiAl-CT catalysts. The superior activity could be attributed to the good dispersion of active phases stemmed from homogeneous elemental distributions of hydrotalcite.

The DMF yields decreased with the decrease of calcination temperature of catalysts. Among the catalysts, NiAl-850 exhibited the highest DMF yield of ~91.5% while NiAl-300 showed the lowest DMF yield of ~44.6%. The byproducts mainly contained the over-hydrogenated product (DMTHF) and the O-containing intermediates (MFA and DHMF). DHMTHF existed with small amount (3–5%) for all catalysts which might be mainly formed during the temperature-rising period.<sup>20</sup> Besides, 2,5-HeD was formed over NiAl-850 and NiAl-750 catalysts.

It is generally concluded that metal-acid bifunctional catalysts are good candidates in hydrogenation/hydrogenolysis reaction, where acid promotes dehydration of CH<sub>2</sub>-OH and metal acts as active phase to saturate/hydrogenate intermediates.<sup>32, 41</sup> For example, Ni-W<sub>2</sub>C/AC bifunctional catalyst with Lewis acid sites could catalyze deoxygenation of HMF to DMF with high efficiency.<sup>19</sup> For NiAl-300 catalyst, large proportions of MFA and DHMF were formed, which suggested the insufficient

deoxygenation ability of the catalyst. NiAl-300 catalyst exhibited the highest amounts of metal sites and lowest amounts of acid sites (Figure 7). Thus, the low DMF yield of NiAl-300 was attributed to the small amount of acid sites. Only 2.8% selectivity of MFA was detected for NiAl-450 and NiAl-600 catalysts, indicating the promoted hydrogenolysis ability due to the enhanced acid concentrations. However, the overhydrogenated product (DMTHF) lowered the DMF yield for NiAl-450, NiAl-600 and NiAl-750 catalysts, which was generated by the saturation of furan ring of DMF. The production of DMTHF indicated the good activity and excessive active Ni sites of these catalysts, which was also in accordance with the results of Figure 7. Besides, 2,5-HeD was formed due to the acid-catalyzed hydrolysis of DMF<sup>42</sup> over NiAl-750 and NiAl-850 catalysts, indicating the sufficient acidity of both catalysts.

To further demonstrate the relationship between metal-acid sites and product distributions, the product selectivities under similar conversions were compared (Table S1). Due to the high reactivity of NiAl-CT catalysts, the catalyst amount was reduced. The similar conversions were obtained by tuning reaction time. NiAl-300, NiAl-750 and NiAl-850 catalysts exhibited high selectivity to DHMF, indicating the weak hydrogenolysis ability of C-O bonds. The DMF selectivity increased firstly and then decreased. Among the catalysts, NiAl-450 showed the highest DMF selectivity, indicating the high amounts of Ni and acid sites. Besides, although HMF conversion of NiAl-600 was lower than NiAl-300, NiAl-600 exhibited similar DMF selectivity with NiAl-300 catalyst, further supporting the role of acid sites. The above results indicated that sole metallic Ni sites or acid sites were hard to convert HMF to DMF efficiently, whereas the balanced Ni-acid sites can facilitate the production of DMF. Besides, the excessive metal sites would promote hydrogenation of C=C bonds (e.g., NiAl-450) to form ring saturated products. The results rationalized the highest DMF yield over NiAl-850 catalyst under the typical conditions (Table 2).

### Synthesis of DMTHF by HMF hydrogenation

DMTHF is also a good candidate for liquid fuel.<sup>12</sup> It could be obtained by saturation of the furan ring of DMF.<sup>20</sup> DMTHF synthesis can be obtained by further tuning reaction conditions (e.g., reaction time) based on DMF synthesis. The time course of HMF hydrogenation over NiAl-850 catalyst was therefore performed (Figure 9) to obtain a high DMTHF yield. With increase of reaction time, DMF yield decreased while DMTHF yield increased monotonically. Finally, a DMTHF yield of 97.4% was obtained over NiAl-850 catalyst after 20 h. The performance of NiAl-CT catalysts was also compared at 20 h (Table 3). The HMF was totally converted into DMTHF and C-C cracking

products (mainly composed of alkanes with different carbon numbers) for all catalysts at these current reaction conditions. Among them, NiAl-850 exhibited the highest DMTHF yield up to 97.4% while the NiAl-450 showed the lowest yield of 80.7%. The results indicated that both the balanced surface sites and the reaction conditions play key roles in achieving good product (DMF and DMTHF) yields.

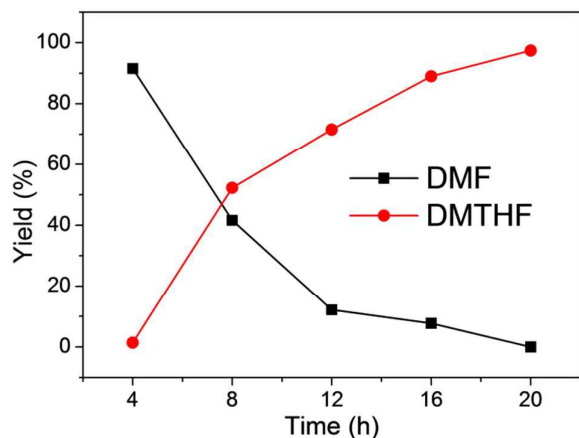


**Figure 9** DMF and DMTHF yield as a function of reaction time over NiAl-850 catalyst. Reaction conditions: 1.2 MPa, 180 °C, HMF 1.5 g, 1,4-dioxane 35 ml, catalyst 0.1 g.

**Table 3** Hydrogenation of HMF over NiAl-CT catalysts.<sup>a</sup>

Catalyst	Conv. %	Sel. %		
		DMTHF	DMF	Others
NiAl-850	100	97.4	0	2.6
NiAl-750	100	94.6	0	5.4
NiAl-600	100	82.2	0	17.8
NiAl-450	100	80.7	0	19.3
NiAl-300	100	87.2	0	12.8

<sup>a</sup> Reaction conditions: 1.2 MPa, 180 °C, 20 h, HMF 1.5 g, 1,4-dioxane 35 ml, catalyst 0.1 g. Others mainly include tetrahydrofuran and C-C cracking products.

### Synthesis of DHMTHF by HMF hydrogenation

DHMTHF is a promising monomer in the manufacture of polyesters and a precursor for 1,6-hexanediol synthesis.<sup>43</sup> To produce DHMTHF, the aldehyde group and furan ring of HMF need to be saturated without further hydrogenolysis of side hydroxymethyl groups. DHMF was the intermediate for DHMTHF synthesis. Low reaction temperature would benefit the DHMTHF selectivity and suppress the side reactions (e.g., C-O hydrogenolysis).<sup>20</sup> High H<sub>2</sub> pressure was also advantageous in terms of DHMTHF yield.<sup>22</sup> In our case, the tests were then performed at 60 °C and 6 MPa.

As shown in **Table 4**, NiAl-300 and NiAl-450 both exhibited 100% conversion and high DHMTHF selectivity (>90%) due to the high dispersions of Ni sites and proper reaction conditions. For catalysts calcined at high temperatures, the HMF conversion and DHMTHF selectivity

were lower than those of NiAl-300 and NiAl-450 catalysts, indicating the insufficient hydrogenation ability of catalysts. This could be attributed to the decrease of surface Ni sites as revealed in **Figure 7**.

**Table 4** Hydrogenation of HMF over NiAl-CT catalysts.<sup>a</sup>

Catalyst	Conv. %	Sel. %		
		DHMTHF	DHMF	Others
NiAl-850	91.2	61.7	38.2	0.1
NiAl-750	91.8	62.0	37.8	0.2
NiAl-600	94.0	75.4	24.4	0.2
NiAl-450	100.0	96.2	3.6	0.2
NiAl-300	100.0	90.5	9.4	0.1

<sup>a</sup> Reaction conditions: 6 MPa, 60 °C, 6 h, HMF 1.5 g, 1,4-dioxane 35 ml, catalyst 0.2 g.

Our results showed the interests to use binary hydrotalcite-like NiAl precursor to prepare metal-acid bifunctional catalysts with controlled surface sites and catalytic performances in terms of both activity and chemo-selectivity. Three broad products including DMF, DMTHF and DHMTHF can be efficiently and selectively synthesized over the well-balanced metal-acid sites and proper reaction conditions. The results also confirmed the potential of non-noble Ni catalysts for HMF hydrogenation.

### Reusability of NiAl-CT catalysts

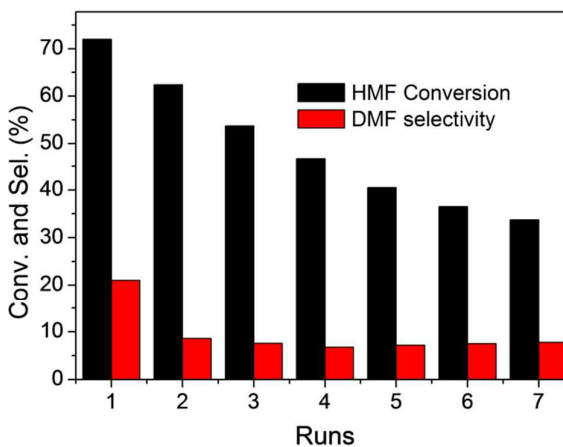


**Figure 10** Reusability of NiAl-850 catalyst for HMF hydrogenation to DMF; Reaction conditions: 1.2 MPa, 180 °C, 2 h, HMF 1.5 g, 1,4-dioxane 35 ml, catalyst 0.05 g.

Among the above reactions, HMF hydrogenation to DMF over NiAl-850 catalyst was chosen to further investigate the reusability of the catalyst due to the relatively severe reaction conditions. In order to better track slight changes in catalyst activity over time, we used relatively mild reaction conditions (180 °C and 2 h) for the hydrogenation of HMF to DMF through 7 cycles of catalysis (**Figure 10**). HMF conversion was around 72.0% with the DMF yield of 21.0% in the first



run. The O-containing intermediates (DHMF and MFA) were the main byproducts. After 7 runs, HMF conversion decreased to 33.7% while the selectivity of DMF reduced to 7.8%. This indicated that the catalyst deactivated during the tests.

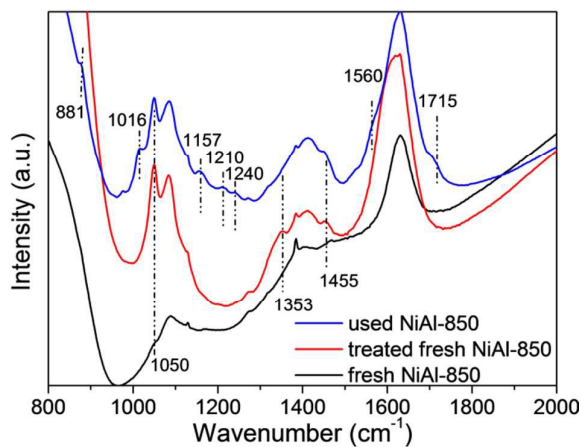


**Figure 11** FT-IR spectra of used NiAl-850, treated fresh NiAl-850 and fresh NiAl-850 catalysts.

The loss of reactivity was probably caused by the formation of high molecular weight impurities during the reaction, which adsorbed on the active sites, as detailed in previous reports.<sup>17,21</sup> Our FT-IR results also supported the formation of carbonaceous species in the used catalyst. The fresh NiAl-850 catalyst and that treated in 1,4-dioxane solvent were employed as the references (**Scheme S1**). As shown in **Figure 11**, several new bands at 1353, 1455 and 1050  $\text{cm}^{-1}$  emerged over treated fresh NiAl-850 catalyst, which are assigned to O-C-H, H-C-H bending and C-O stretching vibration modes of 1,4-dioxane respectively.<sup>44</sup> The used NiAl-850 catalyst exhibited more peaks than treated fresh NiAl-850 catalyst. The peaks at 1016  $\text{cm}^{-1}$  (furan ring breathing) and 881  $\text{cm}^{-1}$  (substituted furan ring) of the used NiAl-850 revealed the adsorption of furan compounds.<sup>45</sup> The peak at 1560  $\text{cm}^{-1}$  could be attributed to the  $\text{C}=\text{C}$  stretching in cyclic compounds while the broad peak at 1715  $\text{cm}^{-1}$  was assigned to  $\text{C}=\text{O}$  bond symmetrical stretching.<sup>46</sup> The vibrational transitions at 1157, 1210 and 1240  $\text{cm}^{-1}$  might be corresponded to stretching vibrations involving the C-H groups and the other substituents bonded to the carbon.<sup>47</sup> The emergence of the above peaks indicated the adsorption of organic compounds over the catalyst surface. TG results further confirmed the observations of FT-IR experiments. As shown in **Figure S4**, the weight of the fresh NiAl-850 catalyst increased, which should be ascribed to the Ni oxidation. In contrast, the weight loss of used NiAl-850 catalyst was obvious around 345  $^{\circ}\text{C}$ , accompanied by a sharp exothermic peak on the heat flow profile, indicating the oxidation of organic compounds (about ~7% content in the used catalyst). Evidently, some carbonaceous species strongly adsorbed on the NiAl-850 catalyst and could not be removed by washing and dry treatments.

The XRD results of used NiAl-850 catalyst showed slight NiO diffractions, indicating the reduction of NiO species during the reaction (**Figure S5**). The intensity of Ni diffractions was not increased in compared with treated fresh NiAl-850, indicating that Ni particles were not grown evidently. The results indicated the good resistance ability of Ni against sintering. During the recycling tests, some catalyst would be inevitably remained on the walls of beakers and centrifuge tubes. Thus, the catalytic performance would be

also influenced by the weight loss of catalyst. The above results suggested that deactivation in our case may be mainly resulted from deposition of carbonaceous species and weight loss of catalyst. Detailed investigation on the regeneration of catalyst will be addressed in our future work.

## Conclusions

In summary, a highly active Ni-Al<sub>2</sub>O<sub>3</sub> catalyst derived from hydrotalcite-like compound was employed for hydrogenation/hydrogenolysis reaction of HMF. The homogeneous elemental distribution of precursor results in the highly dispersed Ni and Al<sub>2</sub>O<sub>3</sub> species; and thus leads to high reactivity of catalysts. The structural properties, surface metallic Ni and acid sites, interactions between active phases and catalytic performance of the catalysts can be finely modulated by tuning calcination temperatures. Striking in this work is that DMF, DMTHF and DHMTHF could be achieved with high yields (91.5%, 97.4% and 96.2% respectively), indicating the potential of Ni-Al<sub>2</sub>O<sub>3</sub> as a promising catalyst for upgradation of biomass. The tunable selectivity of products was achieved by the balanced surface sites and proper reaction conditions. The results also indicate a catalyst design strategy for selective conversion of  $\text{C}=\text{O}$ ,  $\text{C}=\text{C}$ ,  $\text{C}-\text{O}$  bonds, according to different intentions of reactions. Further studies to explore the performances of catalysts with low Ni content and the multi-functionalized catalysts are under progress.

## Acknowledgements

This work was supported by the Major State Basic Research Development Program of China (973 Program, No. 2012CB215305). We also thank Dr. Hongyan Zheng for the helpful suggestions.

## Experimental Section

**Catalyst preparation:** The hydrotalcite-like precursor was prepared by constant-pH co-precipitation method employing NaOH/Na<sub>2</sub>CO<sub>3</sub> as precipitating agent.<sup>27</sup> An aqueous solution containing the Ni(NO<sub>3</sub>)<sub>2</sub>·6H<sub>2</sub>O and Al(NO<sub>3</sub>)<sub>3</sub>·9H<sub>2</sub>O and a solution containing Na<sub>2</sub>CO<sub>3</sub> and NaOH were simultaneously added to flask under vigorous stirring and constant temperature. The Ni/Al molar ratio in solution was 3:1. The precipitate was kept in suspension at 63  $^{\circ}\text{C}$  for 18 h. Then the precipitate was filtered, washed with distilled water and then dried at 63  $^{\circ}\text{C}$  for 24 h. A green material was received and denoted as NiAl-HT. The precursor was calcined at different temperatures in air. The calcined products were denoted as NiAl-CT, where CT represents the calcination temperature. Prior to the tests, the calcined catalysts were reduced in pure H<sub>2</sub> flow at 500  $^{\circ}\text{C}$  for 2 h.

**Catalyst characterization:** Thermo-gravity experiments were acquired using a thermal analysis system (METTLER TOLEDO TGA/SDTA851). The IR spectra were recorded on Nicolet NEXUS 470. The ICP experiments were conducted on PerkinElmer Optima2100DV. The BET surface area was tested via N<sub>2</sub> physical adsorption at -196  $^{\circ}\text{C}$  by a Micromeritics ASAP 2420 instrument. XRD patterns were recorded by a X-ray diffractometer (MiniFlex II, Rigaku) with Cu  $\alpha$  radiation operating at 40 kV, with a rate of 4  $^{\circ}\text{C}/\text{min}$ . Temperature programmed reduction (TPR) was conducted on a Tianjin XQ TP-5080 instrument equipped with a TCD detector. The Raman spectra of the catalysts were measured with a LabRAM HR800 system equipped with a CCD detector. The H<sub>2</sub> temperature programmed desorption (H<sub>2</sub>-

TPD) and CO temperature programmed desorption (CO-TPD) were performed on a Tianjin XQ TP-5080 instrument. Temperature programmed desorption of NH<sub>3</sub> (NH<sub>3</sub>-TPD) experiments were conducted on the AutoChem II. 2920 instrument (Micromeritics, USA) equipped with a mass spectrum detector. (See supporting information for details about the characterizations).

**Catalyst tests:** The tests were performed over a 100 mL tank reactor. For a typical procedure, the reactor was fed with HMF (1.5 g), NiAl-CT and 1,4-dioxane (35 mL), then sealed and purged by H<sub>2</sub> (5 times). After that, the reactor was filled with H<sub>2</sub> in desired pressure and heated to objective temperature. After the test, the reactor was quenched in ice-water, and then the liquid and gas products were analysed by a GC instrument with a FID detector.

## Notes and references

<sup>a</sup> State Key Laboratory of Coal Conversion, Institute of Coal Chemistry, Chinese Academy of Sciences, Taiyuan 030001, PR China.

E-mail: zhuyulei@sxicc.ac.cn (Y. Zhu)

<sup>b</sup> University of Chinese Academy of Sciences, Beijing 100039, PR China.

<sup>c</sup> College of Science, Sichuan Agricultural University, Ya'an 625014, PR China.

<sup>d</sup> Synfuels China Co. Ltd, Beijing, 101407, PR China.

† Electronic Supplementary Information (ESI) available: See DOI: 10.1039/b000000x/

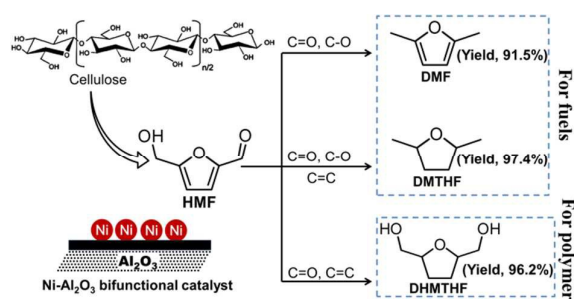
- J. Carlos, Serrano-Ruiz and J. A. Dumesic, *Energy Environ. Sci.*, 2011, **4**, 83-89.
- A. J. Ragauskas, C. K. Williams, B. H. Davison, G. Britovsek, J. Cairney, C. A. Eckert, W. J. Frederick, J. P. Hallett, D. J. Leak and C. L. Liotta, *Science*, 2006, **311**, 484-489.
- N. Shi, Q. Liu, Q. Zhang, T. Wang and L. Ma, *Green Chem.*, 2013, **15**, 1967-1974; J. N. Chheda, Y. Roman-Leshkov and J. A. Dumesic, *Green Chem.*, 2007, **9**, 342-350.
- X. Tong, Y. Ma and Y. Li, *Appl. Catal. A: Gen.*, 2010, **385**, 1-13.
- R.-J. van Putten, J. C. van der Waal, E. de Jong, C. B. Rasrendra, H. J. Heeres and J. G. de Vries, *Chem. Rev.*, 2013, **113**, 1499-1597.
- C. Carlini, P. Patrono, A. M. R. Galletti, G. Sbrana and V. Zima, *Appl. Catal. A: Gen.*, 2005, **289**, 197-204.
- F. M. A. Geilen, T. vom Stein, B. Engendahl, S. Winterle, M. A. Liauw, J. Klankermayer and W. Leitner, *Angew. Chem. Int. Ed.*, 2011, **50**, 6831-6834.
- P. Che, F. Lu, J. Zhang, Y. Huang, X. Nie, J. Gao and J. Xu, *Bioresour. Technol.*, 2012, **119**, 433-436.
- Y. Román-Leshkov, C. J. Barrett, Z. Y. Liu and J. A. Dumesic, *Nature*, 2007, **447**, 982-985.
- T. Thananathanachon and T. B. Rauchfuss, *Angew. Chem. Int. Ed.*, 2010, **122**, 6766-6768.
- M. R. Grochowski, W. Yang and A. Sen, *Chem. Eur. J.*, 2012, **18**, 12363-12371.
- W. Yang and A. Sen, *ChemSusChem*, 2010, **3**, 597-603.
- H. Cai, C. Li, A. Wang and T. Zhang, *Catal. Today*, 2014, **234**, 59-65; Y. Nakagawa and K. Tomishige, *Catal. Commun.*, 2010, **12**, 154-156.
- R. Alamillo, M. Tucker, M. Chia, Y. Pagán-Torres and J. Dumesic, *Green Chem.*, 2012, **14**, 1413-1419.
- G.-H. Wang, J. Hilgert, F. H. Richter, F. Wang, H.-J. Bongard, B. Spliethoff, C. Weidenthaler and F. Schüth, *Nat. Mater.*, 2014, **13**, 293-300.
- Y. Zu, P. Yang, J. Wang, X. Liu, J. Ren, G. Lu and Y. Wang, *Appl. Catal. B: Environ.*, 2014, **146**, 244-248; J. Jae, W. Zheng, A. M. Karim, W. Guo, R. F. Lobo and D. G. Vlachos, *ChemCatChem*, 2014, **6**, 848-856; J. Jae, W. Q. Zheng, R. F. Lobo and D. G. Vlachos, *ChemSusChem*, 2013, **6**, 1158-1162.
- S. Nishimura, N. Ikeda and K. Ebitani, *Catal. Today*, 2013, **232**, 89-98; D. Scholz, C. Aellig and I. Hermans, *ChemSusChem*, 2014, **7**, 268-275; J. Mitra, X. Zhou and T. Rauchfuss, *Green Chem.*, 2014, **17**, 307-313.
- A. J. Kumalaputri, G. Bottari, P. M. Erne, H. J. Heeres and K. Barta, *ChemSusChem*, 2014, **7**, 2266-2275; T. S. Hansen, K. Barta, P. T. Anastas, P. C. Ford and A. Riisager, *Green Chem.*, 2012, **14**, 2457-2461.
- Y. B. Huang, M. Y. Chen, L. Yan, Q. X. Guo and Y. Fu, *ChemSusChem*, 2014, **7**, 1068-1072.
- X. Kong, Y. Zhu, H. Zheng, F. Dong, Y. Zhu and Y.-W. Li, *RSC Adv.*, 2014, **4**, 60467-60472.
- J. Chen, F. Lu, J. Zhang, W. Yu, F. Wang, J. Gao and J. Xu, *ChemCatChem*, 2013, **5**, 2822-2826.
- Y. Nakagawa, K. Takada, M. Tamura and K. Tomishige, *ACS Catal.*, 2014, **4**, 2718-2726.
- Y. Nakagawa, M. Tamura and K. Tomishige, *ACS Catal.*, 2013, **3**, 2655-2668.
- O. Clause, B. Rebours, E. Merlen, F. Trifiro and A. Vaccari, *J. Catal.*, 1992, **133**, 231-246.
- L. Zhao, X. Li, C. Hao and C. L. Raston, *Appl. Catal. B: Environ.*, 2012, **117**, 339-345.
- G. Bonura, M. Cordaro, C. Cannilla, F. Arena and F. Frusteri, *Appl. Catal. B: Environ.*, 2014, **152-153**, 152-161.
- J. Pérez-Ramírez, G. Mul and J. Moulijn, *Vib. Spectrosc.*, 2001, **27**, 75-88.
- M. Jitianu, A. Jitianu, M. Zaharescu, D. Crisan and R. Marchidan, *Vib. Spectrosc.*, 2000, **22**, 75-86.
- B. Vos, E. Poels and A. Bliiek, *J. Catal.*, 2001, **198**, 77-88.
- A. V. Ghule, K. Ghule, S.-H. Tzing, T. H. Punde, H. Chang and Y. C. Ling, *J. Solid State Chem.*, 2009, **182**, 3406-3411; S. S. Chan and I. E. Wachs, *J. Catal.*, 1987, **103**, 224-227.
- M. Jitianu, M. Bălăsoiu, R. Marchidan, M. Zaharescu, D. Crisan and M. Craiu, *Int. J. Inorg. Mater.*, 2000, **2**, 287-300.
- Y. Zhu, X. Kong, X. Li, G. Ding, Y. Zhu and Y.-W. Li, *ACS Catal.*, 2014, **4**, 3612-3620.
- Z. Yuan, L. Wang, J. Wang, S. Xia, P. Chen, Z. Hou and X. Zheng, *Appl. Catal. B: Environ.*, 2011, **101**, 431-440.
- C. Rudolf, B. Dragoi, A. Ungureanu, A. Chiriac, S. Royer, A. Nastro and E. Dumitriu, *Catal. Sci. Tech.*, 2014, **4**, 179-189.
- Y. Zhu, X. Kong, S. Zhu, F. Dong, H. Zheng, Y. Zhu and Y.-W. Li, *Appl. Catal. B: Environ.*, 2015, **166-167**, 551-559.
- F. Prinetto, G. Ghiotti, R. Durand and D. Tichit, *J. Phys. Chem. B*, 2000, **104**, 11117-11126; M. Del Arco, C. Martin, I. Martin, V. Rives and R. Trujillano, *Spectrochim. Acta.*, 1993, **49**, 1575-1582.

37. Y. Zhu, Y. Zhu, G. Ding, S. Zhu, H. Zheng and Y. Li, *Appl. Catal. A: Gen.*, 2013, **468**, 296-304.
38. Y. H. Hu and E. Ruckenstein, *J. Catal.*, 1996, **163**, 306-311.
39. F. Arena, F. Frusteri and A. Parmaliana, *Appl. Catal. A: Gen.*, 1999, **187**, 127-140.
40. C. Park and M. A. Keane, *J. Catal.*, 2004, **221**, 386-399.
41. Y. Kusunoki, T. Miyazawa, K. Kunimori and K. Tomishige, *Catal. Commun.*, 2005, **6**, 645-649.
42. N. Nikbin, S. Caratzoulas and D. G. Vlachos, *ChemSusChem*, 2013, **6**, 2066-2068.
43. T. Buntara, S. Noel, P. H. Phua, I. Melián - Cabrera, J. G. de Vries and H. J. Heeres, *Angew. Chem. Int. Ed.*, 2011, **50**, 7083-7087.
44. K. Mizuno, S. Imafuji, T. Fujiwara, T. Ohta and Y. Tamiya, *J. Phys. Chem. B*, 2003, **107**, 3972-3978.
45. Y. L. Liu and C. Y. Hsieh, *J. Polym. Sci. Pol. Chem.*, 2006, **44**, 905-913; A. Gandini, D. Coelho, M. Gomes, B. Reis and A. Silvestre, *J. Mater. Chem.*, 2009, **19**, 8656-8664.
46. M. Pakuła, A. Świątkowski, M. Walczyk and S. Biniak, *Colloid Surf. A-Physicochem. Eng. Asp.*, 2005, **260**, 145-155; H. Yang, R. Yan, H. Chen, D. H. Lee and C. Zheng, *Fuel*, 2007, **86**, 1781-1788.
47. P. Hellström, S. Öberg, A. Fredriksson and A. Holmgren, *Spectrochim. Acta, Part A*, 2006, **65**, 887-895.

# Rational Design of Ni-based Catalysts derived from Hydrotalcite for Selective Hydrogenation of 5-Hydroxymethylfurfural

Xiao Kong,<sup>a, b</sup> Runxiao Zheng,<sup>c</sup> Yifeng Zhu,<sup>a, b</sup> Guoqiang Ding,<sup>d</sup> Yulei Zhu<sup>\*a, d</sup> and Yong-Wang Li<sup>a, d</sup>

## Table of contents



Hydrotalcite-derived Ni-Al<sub>2</sub>O<sub>3</sub> catalyst can catalyze HMF hydrogenation to DMF, DMTHF and DHMTHF with high yields (91.5%, 97.4% and 96.2% respectively).